京都大学学術情報リポジトリ
KURENAI 紅
Kyoto University Research Information Repository

京都大学
KYOTO UNIVERSITY

| | |
|---|---|
| Title | Impacts of global warming on extreme rainfall of a slow-moving typhoon: A case study for Typhoon Talas (2011) |
| Author(s) | Takemi, Tetsuya |
| Citation | SOLA (2019), 15: 125-131 |
| Issue Date | 2019 |
| URL | http://hdl.handle.net/2433/245854 |
| Right | © The Author(s) 2019. This is an open access article published by the Meteorological Society of Japan under a Creative Commons Attribution 4.0 International (CC BY 4.0) license. |
| Type | Journal Article |
| Textversion | publisher |

Kyoto University

# Impacts of Global Warming on Extreme Rainfall of a Slow-Moving Typhoon: A Case Study for Typhoon Talas (2011)

Tetsuya Takemi
*Disaster Prevention Research Institute, Kyoto University, Uji, Japan*

## Abstract

This study investigated the impacts of global warming on extreme rainfall produced by a slow-moving typhoon by conducting pseudo-global warming (PGW) experiments. We examined Typhoon Talas (2011) that caused long-lasting heavy rainfall exceeding 2000 mm over the Kii Peninsula. The experiments successfully captured the track and translation speed of the actual typhoon, which enabled to quantitatively assess the climate change impacts. The PGW experiments indicated that the extreme rainfall is intensified in the future climates than in the present climate. Especially, the higher extremes of the accumulated rainfall are projected to be more severe in the future climate scenario. The analysis on the environmental factors showed that the cases with increased precipitable water lead to the increases in rainfall in future climates, despite the stabilized atmospheric conditions. Among the PGW experiments, the most increased amount of rainfall was found not to be produced by the most intensified typhoon.

(**Citation**: Takemi, T., 2019: Impacts of global warming on extreme rainfall of a slow-moving typhoon: A case study for Typhoon Talas (2011). *SOLA*, **15**, 125−131, doi:10.2151/sola.2019-023.)

## 1. Introduction

Tropical cyclones (TCs) are one of the most threatening meteorological hazards. Not only wind-induced hazards such as storm surge/high waves and strong gusts as seen in Typhoon Jebi (2018) (Takemi et al. 2019) but also rain-induced hazards are critical. Recently, typhoon-induced extreme rainfall events occurred in the western North Pacific region. Typhoon Morakot (2009) produced record-breaking extreme rainfall, exceeding 3000 mm, over southern Taiwan and spawned devastating damages in the region. Typhoon Talas (2011) generated torrential rainfall exceeding 2000 mm and caused widespread landslides over the Kii Peninsula, Japan. The Philippines are frequently affected by extreme rain events by typhoons. Preventing and mitigating typhoon disasters are one of the major societal concerns in the region.

The maximum intensity of extreme-rain-producing typhoons is not necessarily so severe. Chien and Kuo (2011) indicated that the amount of total rainfall by typhoons affecting Taiwan is inversely proportional to their translation speed. They showed that the very slow movement of Typhoon Morakot (2009) caused torrential rainfall through continuous convective development with sustained moisture supply. Extreme rainfall by Morakot was due to its slow translation speed (Wang et al. 2012; Chien 2014) as well as prolonged asymmetric convection (Wang et al. 2012), orographic enhancement (Yu and Cheng 2013), and others. Typhoon Talas (2011) was also a slow-moving storm and produced long-lasting rains for 5 days. Estimating quantitatively rainfall from slow-moving typhoons is important for assessing the disaster risks not only in the present days but also in future warmed climates.

Studies have been conducted to examine the climate-change impacts on typhoons, through regional-scale, pseudo-global warming (PGW) experiments (Mori and Takemi 2016; Takemi et al. 2016a), such as Typhoon Vera (1959) (Takemi et al. 2016b; Kanada et al. 2017a), Mireille (1991) (Takemi et al. 2016c), Songda (2004) (Ito et al. 2016), and Haiyan (2013) (Takayabu et al. 2015). These studies unanimously indicated that those extreme typhoons become stronger under future global warming. It was also found that the global warming impacts may appear differently depending on latitudinal regions. Ito et al. (2016) and Takemi et al. (2016c) suggested the reduction of high winds in northern Japan by Songda and Mireille, while Kanada et al. (2017b) and Nayak and Takemi (2019) showed that rainfall in northern Japan is enhanced in warmed climates in the cases of both Typhoon Chanthu (2016) and Lionrock (2016).

In contrast, the effects of slow-moving typhoons on rainfall under global warming have not been well investigated. Oku et al. (2014) examined the dependence of rainfall patterns due to Typhoon Talas (2011) on its track; however, the impacts of global warming were not investigated. As the recent study by Kossin (2018) indicated that the translation speed of TCs has decreased globally and suggested a linkage between rainfall amounts and TC translation speed, assessing the impacts of climate change on slow-moving TCs is important.

This study investigated the impacts of global warming on the extreme rainfall of Typhoon Talas (2011) by conducting PGW experiments downscaled at the 1-km grid spacing. Through reproducing closely the actual track and translation speed of Talas, we are able to assess quantitatively the climate change impacts on the extreme rainfall.

## 2. Design of numerical experiments

We used the Weather Research and Forecasting (WRF) model Version 3.3.1 (Skamarock et al. 2008) in a realistic mode configured in two computational domains: the outer domain (Domain 1) covering a region of 4875 km by 4150 km in the western North Pacific at the 5-km grid spacing (exactly the same with that used in Takemi et al. (2016b) for Vera (1959)) and the nested domain (Domain 2), two-way interacting with Domain 1, covering the 430 km by 400 km area that includes the Kii Peninsula at the 1-km grid (Fig. 1, and also see Fig. S1). Both domains had 56 vertical levels up to the 20-hPa level, with the interval stretched with height. Physics parameterizations chosen were the same with those used in Takemi et al. (2016b). Although the 5-km grid in Domain 1 may not be sufficient to represent convective development in tropical cyclones, Kanada et al. (2017a) investigated the performance of 5-km-mesh regional models and demonstrated that the structure and evolution of a typhoon is properly represented. Thus, the use of 5-km grid in Domain 1 is validated. The 1-km grid in Domain 2 is intended to resolve convection development over the Kii Peninsula.

The 6-hourly, 1.25°-resolution Japanese 55-year Reanalysis (JRA-55) dataset (Kobayashi et al. 2015) was used as the initial and boundary conditions for the numerical experiments. Unlike Takemi et al. (2016b), we did not insert an artificial vortex as a TC bogus. The spectral nudging for low wave-number components was applied only for winds above the 3-km height in Domain 1 to keep synoptic-scale influences on the simulated typhoons. We change nudging time coefficients ($g$) and wave number ($wn$), because these nudging parameters affect the typhoon track. The reasoning for the choice of these nudging parameters will be

Corresponding author: Tetsuya Takemi, Disaster Prevention Research Institute, Kyoto University, Gokasho, Uji, Kyoto 611-0011, Japan. E-mail: takemi@storm.dpri.kyoto-u.ac.jp.

©The Author(s) 2019. This is an open access article published by the Meteorological Society of Japan under a Creative Commons Attribution 4.0 International (CC BY 4.0) license (http://creativecommons.org/license/by/4.0).

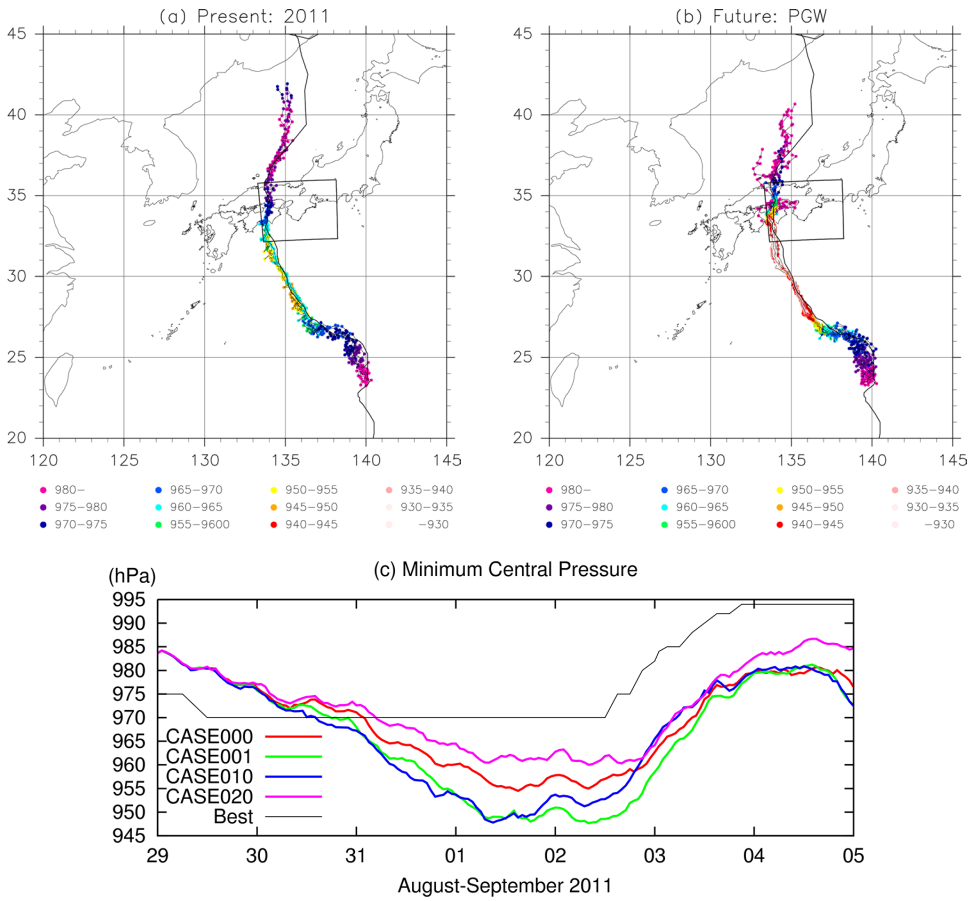


Fig. 1. The track and intensity of Typhoon Talas (2011) (black line) and the simulated typhoons (color points) in (a) the present-climate condition and (b) the PGW conditions. Color points indicate central pressure. The inner black box show the size of Domain 2. (c) The time series of the central surface pressure of the simulated typhoons in the 2011 condition (color lines) as well as the best track (black line).

explained shortly.

In our PGW experiments, the warming increments are defined as the differences, computed as a grid-point basis, averaged in a month both in the present-climate simulation and in the future-climate projection. The global-warming increments here were created from the outputs of the 20-km-mesh MRI-AGCM Version 3.2 (Mizuta et al. 2012) for the present and the future climates under the Representative Concentration Pathway (RCP)-8.5 scenario (Kitoh and Endo 2016). The future climates were driven with the ensemble mean sea surface temperature (SST) averaged for the Coupled Model Intercomparison Project Phase 5 (CMIP5) atmosphere-ocean coupled models and three SST patterns derived from the cluster analysis on the CMIP5 models (Mizuta et al. 2014). The warming increments were defined as the difference in the monthly means of September between the present and the future climates, and the increments of SST, air temperature, and geopotential height were added to the JRA-55 field in 2011, as in Ito et al. (2016), Takemi et al. (2016b, 2016c), and Kanada et al. (2017a). However, the increments of relative humidity and winds were not added, because of no significant change of humidity in the future (Takemi et al. 2012) and difficulty in controlling the typhoon tracks if wind increment is added (Takemi et al. 2016a). The spatial patterns of the warming increments for SST and surface air temperature are found in Takemi et al. (2016b).

By changing the nudging parameters ($wn$, $g$) and the warming increments from the different outputs with the four SST patterns, 4 experiments for the present (2011) condition and 7 experiments for the PGW condition were conducted (Table 1). Because the spectral nudging selectively forces the upper-level winds, with the time coefficient $g$, towards the wind components having horizontal scales larger than the Domain-1 size divided by $wn$, the values of $wn$ and $g$ will change the steering flow of the typhoon. The examined values of $wn$ indicate that the winds are nudged to those with the scales of around 1000 km, while the values of $g$, the reciprocal of 1 or 2 hours, indicate the nudging strength. Therefore, the choice of $wn$ and $g$ is intended to examine the variability

Table 1. The list of the numerical experiments. The future climate data were driven either with the ensemble mean SST averaged for the CMIP5 coupled models (referred to as CNTL) or other different-type SST pattern derived from the cluster analysis on the CMIP5 models (referred to as C1, C2, or C3) (Mizuta et al. 2014). In CNTL, El Niño-type warming is seen in the equatorial Pacific, and warming is larger in the Northern Hemisphere than in the Southern Hemisphere, with the largest SST warming in the northern North Pacific. In C1 smaller warming occurs in the eastern tropical Pacific; in C2 El Niño-type warming in the tropics is more pronounced; in C3 large warming appears in the western North Pacific.

| | Case | wave number $wn$ | time coefficient $g$ | SST in PGW |
|---|---|---|---|---|
| Present climate | CASE000 | 5 | 0.00028 | – |
| | CASE001 | 5 | 0.00014 | – |
| | CASE010 | 4 | 0.00028 | – |
| | CASE020 | 6 | 0.00028 | – |
| PGW climate | CASE100 | 5 | 0.00028 | CNTL |
| | CASE101 | 5 | 0.00014 | CNTL |
| | CASE110 | 4 | 0.00028 | CNTL |
| | CASE120 | 6 | 0.00028 | CNTL |
| | CASE200 | 5 | 0.00028 | C1 |
| | CASE300 | 5 | 0.00028 | C2 |
| | CASE400 | 5 | 0.00028 | C3 |

of steering flow in controlling the typhoon track. By considering the typhoon track variability, we will demonstrate the robustness of the impacts of global warming on typhoon-induced rainfalls in the Kii Peninsula.

We also performed experiments without imposing spectral nudging and found that the typhoon tracks under the actual and PGW conditions were completely different from the best-track and those obtained in the experiments with the nudging, which led to significant reduction of the rainfall in the Kii Peninsula (not shown). This is inappropriate for the impact assessment studies. Takemi (2018) successfully reproduced the track and intensity of a tropical cyclone in the southern Pacific by using the spectral nudging and was able to assess the impact of strong wind hazards at local scales. Therefore, the spectral nudging has to be applied in order to control the typhoon track for assessing local-scale hazards.

All the time integrations were started at 0000 UTC 29 August for Domain 1 and 0000 UTC 31 August for Domain 2 and ended at 0000 UTC 5 September. The model outputs at 1-hour interval were used for the analyses.

## 3. Results

First we will demonstrate the overall performance of the simulations in reproducing the track, intensity, and translation speed of the typhoon.

Figure 1 compares the track and intensity of the simulated typhoons with the best-track data of Japan Meteorological Agency. The simulated typhoon centers were determined with the method of Braun (2002). In the present climate, all the experiments successfully reproduce the actual track; the landfall location is also well simulated. However, the experiments overestimate the maximum intensity: the minimum central pressure is 970 hPa in the best-track, while in the experiments vary between 948−960 hPa (Fig. 1c). Considering the case of Vera (1959) (Takemi et al. 2016b), the difference of about 10−15 hPa is acceptable. In the PGW cases, the experiments also capture well the track and landfall location of the typhoon, with the maximum intensities being stronger (905−938 hPa) than in the present-climate.

Figure 2 shows the northward translation of the simulated typhoons as well as the best-track data. The northward movement of the actual typhoon is well captured in the present-climate experiments. The averaged translation speed of the actual typhoon was 4.2 m $s^{-1}$ from 0000 UTC 30 August to 0000 UTC 3 September; this slow movement was also reproduced well in the PGW experiments. In Oku et al. (2014), the simulated translation speeds were 1.2 to 1.7 times faster than that of the actual case. Thus, this study is successful in closely reproducing the Talas's slow movement.

Next, the simulated rainfalls in the present-climate, computed at grid points nearest to the observation points, are validated against the observations. Figure 3 compares the hourly and accumulated rainfalls at the points in the mountainous area of the Kii Peninsula (see Fig. S1). In the observations the hourly rainfall changes indicate weaker rain in the first 2 days, intensified rain on 2 and 3 September, and ceasing rain on 4 September; these features are generally represented in the experiments. Quantitatively, there are differences between the observations and the experiments, clearly seen in the time series of the accumulated rainfall. For example, at Kamikitayama and Miyagawa the simulated accumulations are only about half of the observed. In contrast, there are experiments that better reproduced the observed accumulation, for example, at Ryujin, Tamakiyama, and Tenkawa in CASE020. By conducting ensemble experiments with nudging parameters changes we were able to obtain results that successfully reproduced the extreme rainfall by the typhoon. Based on this performance, we are going to investigate the influences of global-warming increments on the rainfall in the Kii Peninsula.

The spatial distributions of the total rainfall during the simulated period in the present-climate experiments are demonstrated in Fig. 4. In every case, the total rainfall exceeds 1000 mm in the mountainous areas of the Kii Peninsula. Moreover, the experiments capture the extreme amount exceeding 2000 mm in the eastern part of the region, which is consistent with the radar-gauge analysis rainfall (Oku et al. 2014).

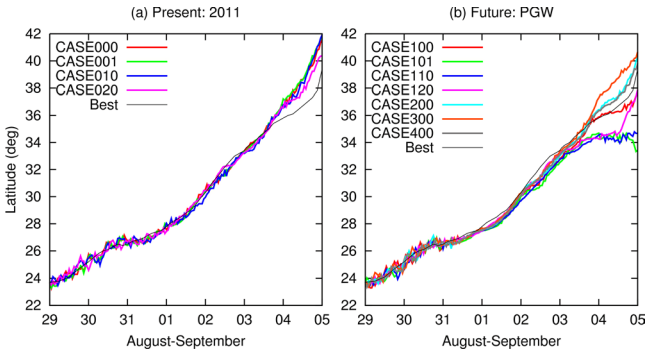


Fig. 2. The temporal change of the latitudinal location of the typhoon center in (a) the present-climate condition and (b) the PGW conditions, as well as the best-track data.

The distributions of the total rainfall in the PGW experiments are exhibited in Fig. 5. The total rainfall is generally higher in the mountainous areas in all the cases. The increased amount of rainfall is clearly seen in CASE101 (Fig. 5b), CASE110 (Fig. 5c), and CASE120 (Fig. 5d), compared with the present-climate counterparts. In these cases the areas of the rainfall exceeding 2000 mm become wider and the peak amounts become more enhanced than in the present-climate cases. The distributions in CASE100 (Fig. 5a), CASE200 (Fig. 5e), CASE300 (Fig. 5f), and CASE400 (Fig. 5g) appear similar with each other and also with the present case of CASE000, but the extreme amounts in the eastern part seem to be increased in the PGW cases.

The changes in rainfall in the different climates are further examined in terms of the hourly intensity and the total amount. Figures 6a, 6b, 6c, and 6d show the cumulative relative frequency distributions of the total and hourly rainfalls over the Kii Peninsula during the simulated period. Although the variability is larger in the PGW cases than in the present-climate ones, clear signatures are found. CASE101, CASE110, and CASE120 indicate higher frequencies in higher values of both the total and hourly rainfalls than the present-climate cases, while CASE100, CASE300, and CASE400 show higher frequencies in lower range of the rainfalls. Focusing on the higher extremes of the rainfalls, the total rainfall in the extremes is seen to be more frequent in all the PGW cases than in the present-climate cases (Fig. 6c), while the rain intensity becomes very severe in some PGW cases (i.e., CASE101, CASE110, and CASE120) than in the present-climate counterparts (Fig. 6d).

To interpret the characteristics of the rainfall changes, we examine environmental factors relevant to convective rainfall. The environments are defined as the properties computed in the region upstream of the Kii Peninsula. Figures 6e and 6f show the cumulative frequency distributions of precipitable water (PW) and temperature lapse rate in the convectively unstable layer of 0.5−5 km heights (Takemi 2007, 2010, 2014). In the PGW conditions, PW becomes larger (because of increased temperature with relative humidity unchanged), while the temperature lapse rate becomes smaller (because of larger temperature increase at higher levels), which is consistent with the previous findings (Santer et al. 2008; Takemi et al. 2012; Takemi 2012). This means that the PGW environment is favorable for convective development in terms of moisture availability but is unfavorable in terms of the atmospheric stability. In CASE200, CASE300, and CASE400, the atmosphere is more stabilized, suppressing the convection even with higher amounts of moisture, than in the present-climate cases. On the other hand, CASE101, CASE110, and CASE120 have more abundant moisture, which promotes convection in the PGW conditions. An exception can be seen for CASE100, which is characterized as having more destabilized and more PW envi-

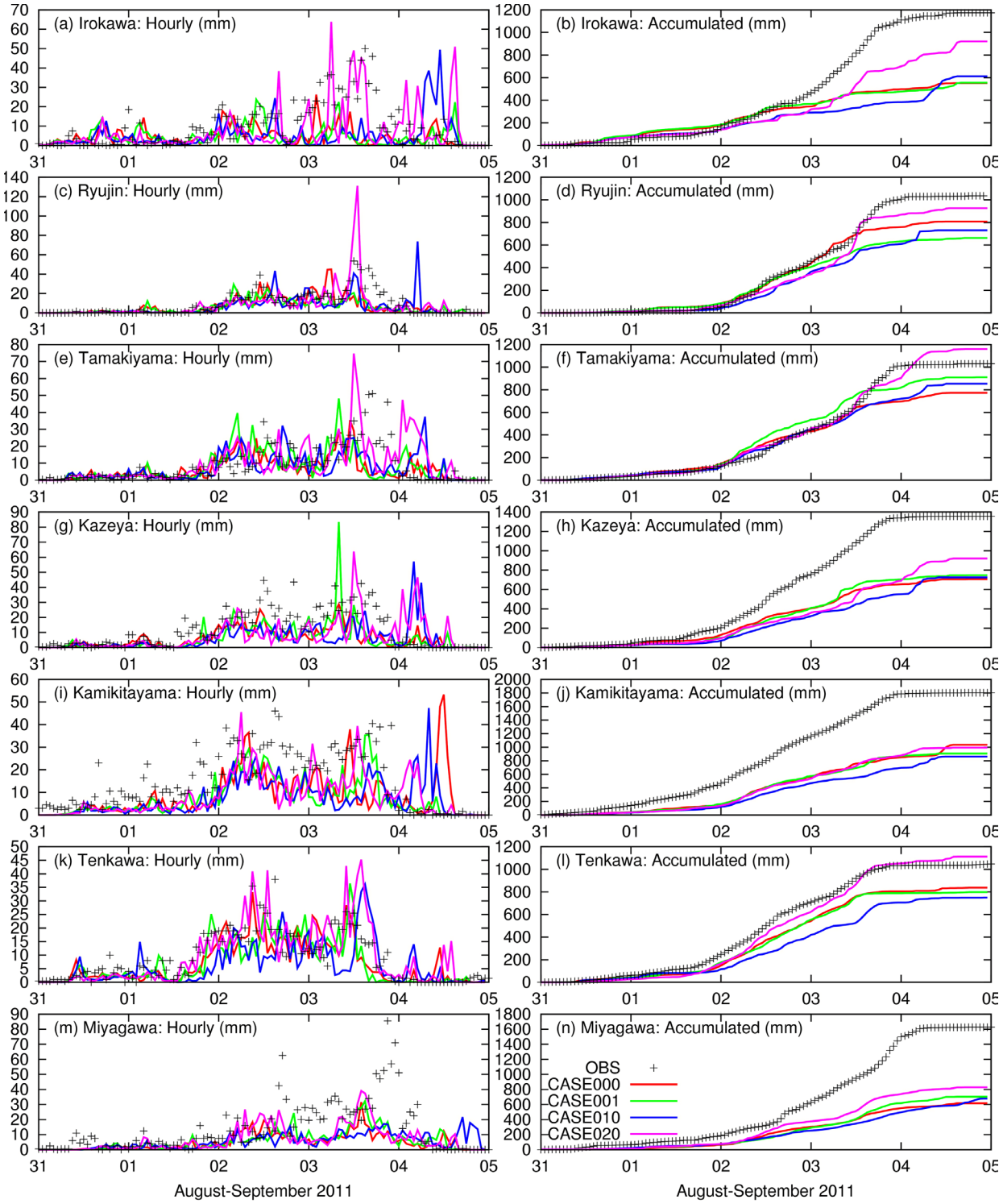


Fig. 3. The time series of hourly and accumulated rainfalls observed at the surface observation sites and simulated at the corresponding grid points in CASE000, CASE001, CASE010, and CASE020. The observation sites chosen were (a) (b) Irokawa (33°40.5′N, 135°50.9′E), (c) (d) Ryujin (33°56.7′N, 135°33.4′E), (e) (f) Tamakiyama (33°55.6′N, 135°49.8′E), (g) (h) Kazeya (34°2.7′N, 135°47.2′E), (i) (j) Kamikitayama (34°8.2′N, 136°0.3′E), (k) (l) Tenkawa (34°16.2′N, 135°53.0′E), and (m) (n) Miyagawa (34°16.7′N, 136°12.5′E).

ronments but less extreme rainfall frequency than the other PGW cases. Comparing the settings between CASE100 and CASE101, the nudging coefficient of CASE100 is larger, keeping the more stable condition of the PGW field; such a background state is determined by the MRI-AGCM future projection runs (Kitoh and Endo 2016). However, the extreme rainfall frequency is still higher in CASE100 than in the present-climate cases. Overall, strong convection will sporadically develop; once convection occurs, the extreme rainfall is generated. This is considered to be why the extreme total rainfall is more significant in all the PGW cases.

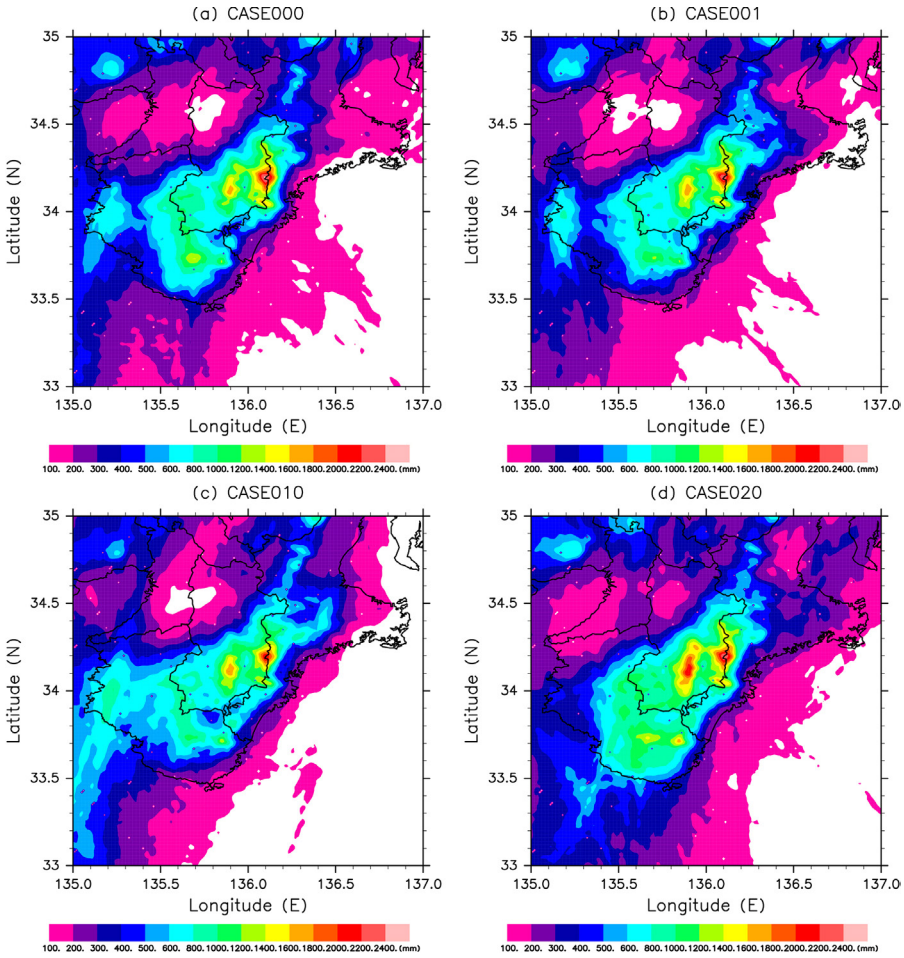


Fig. 4. The accumulated rainfall in Domain 2 during 0000 UTC 31 August and 0000 UTC 5 September for (a) CASE000, (b) CASE001, (c) CASE010, and (d) CASE020.

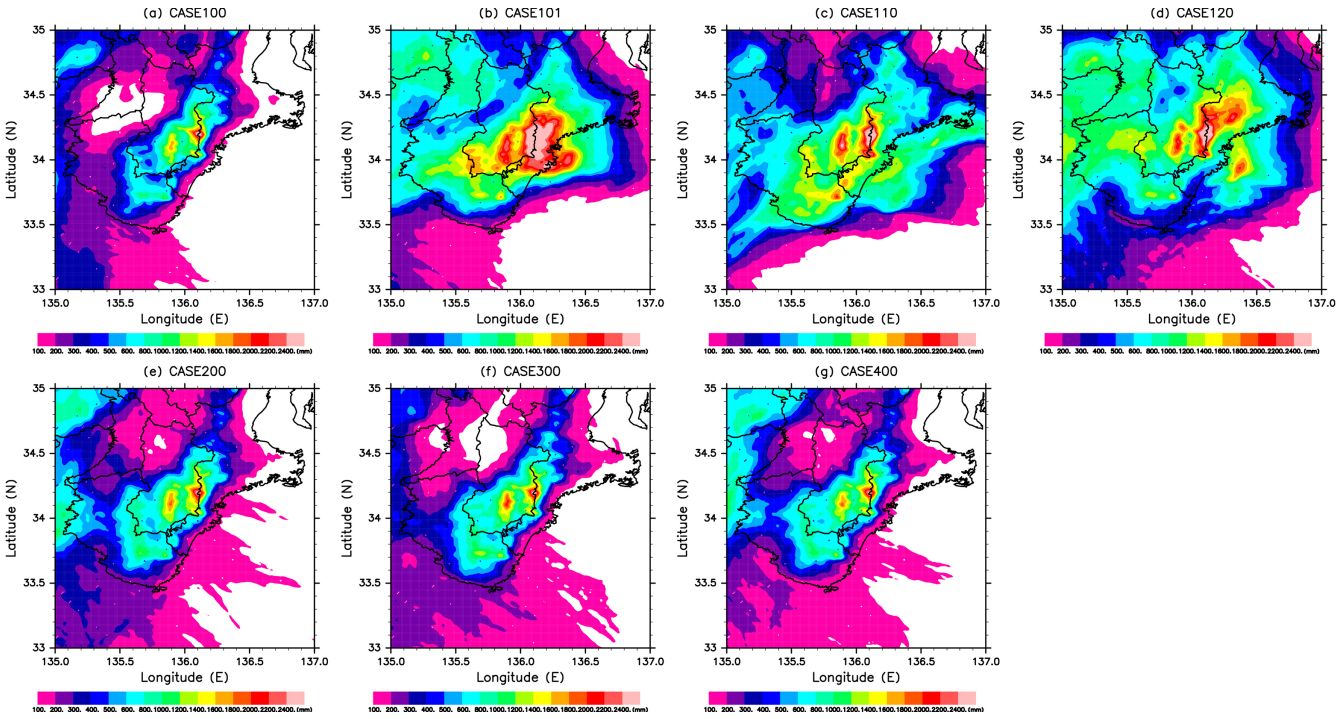


Fig. 5. The same as Fig. 4, but for (a) CASE100, (b) CASE101, (c) CASE110, (d) CASE120, (e) CASE200, (f) CASE300, and (g) CASE400.

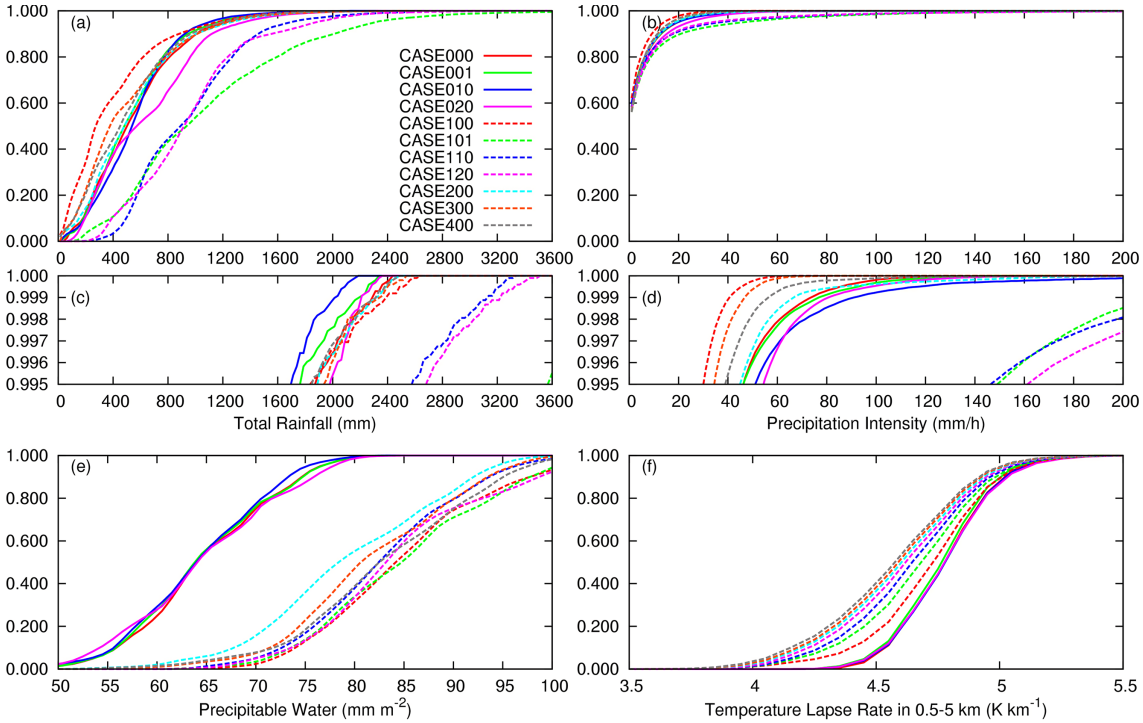


Fig. 6. The cumulative frequency distribution of (a) total rainfall, (b) hourly rainfall, (c) focused on extremes of (a), and (d) focused on extremes of (b) at the grid points over the Kii Peninsula in the south of 34.4°N within Domain 2 during the simulated time period from 0000 UTC 31 August to 0000 UTC 5 September. The cumulative frequency distribution of (e) precipitable water vapor and (f) temperature lapse rate in the layer of 0.5−5 km computed in the region of 135°E−140°E and 28°N−33°N, upstream of the Kii Peninsula, within Domain 2 during the simulated time period.

## 4. Conclusions and discussion

This study investigated, by conducting PGW experiments, the influences of global warming on the extreme rainfall of Typhoon Talas (2011). A unique feature of this typhoon is its slow translation speed and hence prolonged existence to the south of the Kii Peninsula where heavy rainfall exceeding 2000 mm occurred. The track and translation speed of the typhoon were successfully simulated in the present-climate experiments and were reproduced also in the PGW experiments. The PGW experiments produced stronger typhoons with their lifetime minimum central pressure being in the range of 905−938 hPa.

The extreme amount of the total rainfall within the region increases from the present-climate to the PGW conditions. If the higher extremes of the rainfalls are focused, the total rainfall in all the PGW cases indicates a higher frequency than that in the present-climate cases. In some PGW cases, the areas of the rainfall exceeding 2000 mm become wider and the total rainfall generally is more enhanced. In these cases, the hourly rainfall also becomes stronger than in the present-climate cases. The environmental factors affecting these climate change influences indicate competing contributions from increased moisture content (which promotes convection) and decreased instability (which prohibits convection). In some PGW cases that exhibit clearer signature of the increased extreme rainfall, their environmental precipitable water is significantly larger among all the PGW cases. This indicates that in terms of the rainfall impact the positive contribution from increased moisture becomes stronger than the negative contribution from decreased instability. Therefore, with a sufficient amount of moisture, strong convection develops despite an increased stability, leading to extreme rainfall.

The intensified rainfall by typhoons under global warming was demonstrated for typhoons that made landfall not only in the southern side of the Japanese islands (Takemi et al. 2016b) but also in northern Japan (Kadana et al. 2017b; Nayak and Takemi 2019). Thus, it is anticipated that typhoon-induced rainfall will be a more threatening hazard commonly in the mid-latitude region under climate change. Considering that a tendency for the decreased translation speed of TCs emerges (Kossin 2018), the impact of the slow-movement will be an additional factor for future hazards.

This study has successfully simulated the slow translation of the typhoon and the associating extreme rainfall. In general, extreme-rain-producing TCs are not necessarily as strong as super-typhoons having maximum 1-minute sustained winds greater than 65 m $s^{-1}$. We also indicated that the amount of extreme rainfall and the typhoon intensity was not correlated, supporting that rainfall amount is difficult to estimate from the TC intensity solely from the wind-pressure relationships of TCs. TC induced precipitation has a large variability depending on geographical and topographical features (Kamahori and Arakawa 2018). Thus, the significance of the slow-moving TC is that the impacts of global warming will appear remarkably for the total accumulated rainfall despite minor changes in hourly rainfall, because of long-lasting rainfall. Therefore, we conclude that the time duration of rainfall caused by slow-moving typhoons is critical in assessing the impacts on rainfall hazards.

## Acknowledgments

The comments by two anonymous reviewers are greatly acknowledged in improving the manuscript. I would like to thank Drs. Rui Ito and Osamu Arakawa for their help in conducting PGW experiments. This work was supported by the MEXT TOUGOU program and JSPS Kakenhi 16H01846.

Edited by: K. Cheung

## Supplements

Supplement 1: Fig. S1 shows the map of the Kii Peninsula.

## References


Braun, S. A., 2002: A cloud-resolving simulation of Hurricane Bob (1991): Storm structure and eyewall buoyancy. *Mon. Wea. Rev.*, **130**, 1573−1592.

Chien, F. C., 2014: A numerical study on the slow translation speed of Typhoon Morakot (2009). *SOLA*, **10**, 190−193.

Chien, F. C., and H. C. Kuo, 2011: On the extreme rainfall of Typhoon Morakot (2009). *J. Geophys. Res.*, **116**, D05104, doi:10.1029/2010JD015092.

Ito, R., T. Takemi, and O. Arakawa, 2016: A possible reduction in the severity of typhoon wind in the northern part of Japan under global warming: A case study. *SOLA*, **12**, 100−105, doi:10.2151/sola.2016-023.

Kain, J. S., 2004: The Kain-Fritsch convective parameterization: An update. *J. Appl. Meteor.*, **43**, 170−181.

Kamahori, H., and O. Arakawa, 2018: Tropical cyclone induced precipitation over Japan using observational data. *SOLA*, **14**, 165−169, doi:10.2151/sola.2018-029.

Kanada, S., T. Takemi, M. Kato, S. Yamasaki, H. Fudeyasu, K. Tsuboki, O. Arakawa, and I. Takayabu, 2017a: A multi-model intercomparison of an intense typhoon in future, warmer climates by four 5-km-mesh model. *J. Climate*, **30**, 6017−6036.

Kanada, S., K. Tsuboki, H. Aiki, S. Tsujino, and I. Takayabu, 2017b: Future enhancement of heavy rainfall events associated with a typhoon in the midlatitude regions. *SOLA*, **13**, 246−251, doi:10.2151/sola.2017-045.

Kitoh, A., and H. Endo, 2016: Changes in precipitation extremes projected by a 20-km mesh global atmospheric model. *Wea. Climate Extremes*, **11**, 41−52, doi:10.1016/j.wace.2015.09.001.

Kobayashi, S., Y. Ota, Y. Harada, A. Ebita, M. Moriya, H. Onoda, K. Onogi, H. Kamahori, C. Kobayashi, H. Endo, K. Miyaoka, and K. Takahashi, 2015: The JRA-55 Reanalysis: General specifications and basic characteristics. *J. Meteor. Soc. Japan*, **93**, 5−48, doi:10.2151/jmsj.2015-001.

Kossin, J. P., 2018: A global slowdown of tropical-cyclone translation speed. *Nature*, **558**, 104−107, doi:10.1038/s41586-018-0158-3.

Mizuta, R., O. Arakawa, T. Ose, S. Kusunoki, H. Endo, and A. Kitoh, 2014: Classification of CMIP5 future climate responses by the tropical sea surface temperature changes. *SOLA*, **10**, 167−171, doi:10.2151/sola.2014-035.

Mizuta, R., H. Yoshimura, H. Murakami, M. Matsueda, H. Endo, T. Ose, K. Kamiguchi, M. Hosaka, M. Sugi, S. Yukimoto, S. Kusunoki, and A. Kitoh, 2012: Climate simulations using MRI-AGCM3.2 with 20-km grid. *J. Meteor. Soc. Japan*, **90A**, 233−258, doi:10.2151/jmsj.2012-A12.

Mori, N., and T. Takemi, 2016: Impact assessment of coastal hazards due to future changes of tropical cyclones in the North Pacific Ocean. *Wea. Climate Extremes*, **11**, 53−69, doi:10.1016/j.wace.2015.09.002.

Nayak, S., and T. Takemi, 2019: Dynamical downscaling of Typhoon Lionrock (2016) for assessing the resulting hazards under global warming. *J. Meteor. Soc. Japan*, **97**, 69−88, doi:10.2151/jmsj.2019-003.

Oku, Y., J. Yoshino, T. Takemi, and H. Ishikawa, 2014: Assessment of heavy rainfall-induced disaster potential based on an ensemble simulation of Typhoon Talas (2011) with controlled track and intensity. *Nat. Hazards Earth Sys. Sci.*, **14**, 2699−2709, doi:10.5194/nhess-14-2699-2014.

Oku, Y., T. Takemi, H. Ishikawa, S. Kanada, and M. Nakano, 2010: Representation of extreme weather during a typhoon landfall in regional meteorological simulations: A model intercomparison study for Typhoon Songda (2004). *Hydrol. Res. Lett.*, **4**, 1−5, doi:10.3178/hrl.4.1.

Santer, B. D., P. W. Thorne, L. Haimberger, K. E. Taylor, T. M. L. Wigley, J. R. Lanzante, S. Solomon, N. Free, P. J. Gleckler, P. D. Jones, T. R. Karl, S. A. Klein, C. Mears, D. Nychka, G. A. Schmidt, S. C. Sherwood, and F. J. Wentz, 2008: Consistency of modelled and observed temperature trends in the tropical troposphere. *Int. J. Climatol.*, **28**, 1703−1722, doi:10.1002/joc.1756.

Skamarock, W. C., J. B. Klemp, J. Dudhia, D. O. Gill, D. M. Barker, M. G. Duda, X. Y. Huang, W. Wang, and J. G. Powers, 2008: A description of the Advanced Research WRF version 3. NCAR Tech. Note NCAR/TN-475+STR, 113 pp.

Takayabu, I., K. Hibino, H. Sasaki, H. Shiogama, N. Mori, Y. Shibutani, and T. Takemi, 2015: Climate change effects on the worst-case storm surge: A case study of Typhoon Haiyan. *Environ. Res. Lett.*, **10**, 064011, doi:10.1088/1748-9326/10/6/064011.

Takemi, T., 2007: A sensitivity of squall line intensity to environmental static stability under various shear and moisture conditions. *Atmos. Res.*, **84**, 374−389, doi:10.1016/j.atmosres.2006.10.001

Takemi, T., 2010: Dependence of the precipitation intensity in mesoscale convective systems to temperature lapse rate. *Atmos. Res.*, **96**, 273−285, doi:10.1016/j.atmosres.2009.09.002.

Takemi, T., 2012: Projected regional-scale changes in atmospheric stability condition for the development of summertime convective precipitation in the Tokyo metropolitan area under global warming. *Hydrol. Res. Lett.*, **6**, 17−22, doi:10.3178/HRL.6.17.

Takemi, T., 2014: Convection and precipitation under various stability and shear conditions: Squall lines in tropical versus midlatitude environment. *Atmos. Res.*, **142**, 111−123, doi:10.1016/j.atmosres.2013.07.010.

Takemi, T., 2018: The evolution and intensification of Cyclone Pam (2015) and resulting strong winds over the southern Pacific islands. *J. Wind Eng. Ind. Aerodyn.*, **182**, 27−36, doi:10.1016/j.jweia.2018.09.007.

Takemi, T., S. Nomura, Y. Oku, and H. Ishikawa, 2012: A regional-scale evaluation of changes in environmental stability for summertime afternoon precipitation under global warming from super-high-resolution GCM simulations: A study for the case in the Kanto Plain. *J. Meteor. Soc. Japan*, **90A**, 189−212, doi: 10.2151/jmsj.2012-A10.

Takemi, T., Y. Okada, R. Ito, H. Ishikawa, and E. Nakakita, 2016a: Assessing the impacts of global warming on meteorological hazards and risks in Japan: Philosophy and achievements of the SOUSEI program. *Hydrol. Res. Lett.*, **10**, 119−125, doi:10.3178/hrl.10.119.

Takemi, T., R. Ito, and O. Arakawa, 2016b: Robustness and uncertainty of projected changes in the impacts of Typhoon Vera (1959) under global warming. *Hydrol. Res. Lett.*, **10**, 88−94, doi:10.3178/hrl.10.88.

Takemi, T., R. Ito, and O. Arakawa, 2016c: Effects of global warming on the impacts of Typhoon Mireille (1991) in the Kyushu and Tohoku regions. *Hydrol. Res. Lett.*, **10**, 81−87, doi:10.3178/hrl.10.81.

Takemi, T., T. Yoshida, S. Yamasaki, and K. Hase, 2019: Quantitative estimation of strong winds in an urban district during Typhoon Jebi (2018) by merging mesoscale meteorological and large-eddy simulations. *SOLA*, **15**, 22−27, doi:10.2151/sola.2019-005.

Wang, C.-C., H.-C. Kuo, Y.-H. Chen, H.-L. Huang, C.-H. Chung, and K. Tsuboki, 2012: Effects of asymmetric latent heating on typhoon movement crossing Taiwan: The case of Morakot (2009) with extreme rainfall. *J. Atmos. Sci.*, **69**, 3172−3196.

Yu, C.-K., and L.-W. Cheng, 2013: Distribution and mechanisms of orographic precipitation associated with Typhoon Morakot (2009). *J. Atmos. Sci.*, **70**, 2894−2915.


*Manuscript received 23 February 2019, accepted 26 April 2019*
*SOLA: https://www.jstage.jst.go.jp/browse/sola/*